

## Bio-inspired synthesis and optical properties of Dy<sup>3+</sup>-doped ZnS nanoparticles

Xiuying Tian<sup>a,b,\*</sup>, Zhanjun Chen<sup>a,b</sup>, Jin Wen<sup>a,b,\*</sup>, Yi Du<sup>c</sup>, Jilin Hu<sup>a,b</sup>, Shumei Wang<sup>a,b</sup>, Hongxia Peng<sup>a,b</sup>  
and Jing Li<sup>a,b</sup> and Yangxi Peng<sup>a,\*</sup>

<sup>a</sup>Hunan Provincial Key Laboratory of Fine Ceramics and Powder Materials, Hunan University of Humanities, Science and Technology, Loudi, 417000, P. R. China

<sup>b</sup>School of Materials and Environmental Engineering, Hunan University of Humanities, Science and Technology, Loudi, 417000, P. R. China

<sup>c</sup>Shandong Provincial Key Laboratory of Processing and Testing Technology of Glass & Functional Ceramics, School of Materials Science and Engineering, Qilu university of technology, Jinan, 250353, P. R. China

Dy<sup>3+</sup>-doped Zinc sulfide (ZnS) nanoparticles had been prepared via bio-inspired procedure and were characterized. All samples had cubic zinc blende structures. The typical sample had spherical structure with a diameter of ca. 68 nm. With increasing Dy<sup>3+</sup>-doped concentration, the bands attributed to C-O were shifted, due to the presence of Dy<sup>3+</sup> ion in ZnS lattice site. The obtained bandgap were apparently lower than the reference value (~3.72 eV), beneficial for the photo-catalytic application. With increase of Dy<sup>3+</sup>-doped concentrations, enhanced photoluminescence (PL) of the sample at 1% was attributed to large number of sulfur vacancies. The broad band with blue-green emission at ~500 nm indicated a considerable number of zinc vacancies to impart green emission and <sup>4</sup>F<sub>9/2</sub>-<sup>6</sup>H<sub>15/2</sub> transitions of Dy<sup>3+</sup> ions to impart blue emission.

**Key words:** Semiconductors, Crystal growth, Optical properties, X-ray diffraction, Crystal structure.

### Introduction

Semiconductor nanoparticles have attracted widespread attention because of its unique optical and electric properties suitable for applications in gas sensors, ultraviolet detector, photoelectric devices, photocatalysis and luminescence properties [1]. In order to get enhanced emissions of luminescent materials with various wavelength, it is important to synthesize ions-doped semiconductor nanoparticles. Recently, ions-doped semiconductor nanoparticles with applications in sensors, solar cells, photocatalysts and light emitting diodes, have been attracting special attention [2].

ZnS with cubic zinc blende (ZB) and hexagonal Wurtzite (WZ) crystal structure, has band gap energies of ~3.72 and ~3.77 eV at room temperature, respectively [3]. Up to date, ZnS has been investigated as a matrix to synthesize doping nanostructures for enhanced optical properties. Cu<sup>2+</sup>[4], Ag<sup>+</sup>[5], Au<sup>3+</sup>[5], Mn<sup>2+</sup>[6], Fe<sup>3+</sup>[7], Ni<sup>2+</sup>[8], Mg<sup>2+</sup>[9], Pb<sup>2+</sup>[10], Gd<sup>3+</sup>[11], Cd<sup>2+</sup>[12,13], La<sup>3+</sup>[14] Eu<sup>3+/2+</sup>[15,16] and Dy<sup>3+</sup>[17] ions-doped ZnS nanostructures have been obtained. Dy<sup>3+</sup> ion has the yellow band (576 nm) attributed to the hypersensitive transition <sup>4</sup>F<sub>9/2</sub>-<sup>6</sup>H<sub>13/2</sub> and the blue band (484 nm) due to the <sup>4</sup>F<sub>9/2</sub>-<sup>6</sup>H<sub>15/2</sub> transition in the emission spectrum. The factors like the excitation wavelength, host composition

and doping concentration have effect on the intensity ratio of yellow to blue bands [18]. It is possible to investigated luminescent properties from Dy<sup>3+</sup> doped ZnS nanostructures by adjusting the doping concentration. To date, ZnS nanorods [19], nanowires [20], nanosheets [21], nanotubes [22], nanoparticles [23] and flower-like nanostructures [24] have been synthesized via different procedures and systematic techniques. Among various approaches, green synthetic methods have been demonstrated to be appealing for preparing nanostructures [25]. Some nanostructures prepared via bio-template such as yeast, starch, silk, albumen, DNA, wood, β-cyclodextrin, peptide, pollen grain, orange juice, rice, egg-shell membrane and egg albumin have been extensively investigated [26-38]. Starch is one of the most appealing bio-templates for nanoparticles, and has been recommended as a very valuable ingredient for green synthesis due to eco-friendly attributes [39]. As known, microwave irradiation has been applied to form nanoparticles [40]. Up to now, Ag, Cu<sub>2</sub>O and ZnS nanoparticles via starch and microwave-assisted procedure have been reported [39, 41, 42]. However, to our best knowledge, Dy<sup>3+</sup> ions-doped ZnS nanoparticles via starch and microwave-assisted procedure have not been reported.

In this paper, we have aimed at fabrication of Dy<sup>3+</sup> ions-doped ZnS nanoparticles via a microwave and starch-assisted route, as it was simple, inexpensive and more productive. By using XRD, HR-TEM, FE-SEM, FTIR, UV-Vis spectroscopy, and FL spectrometer, the phases, crystalline lattice structure, morphologies, chemical and optical properties are characterized.

\*Corresponding author:  
Tel : +86-0738-8325065  
Fax: +86-0738-8376006  
E-mail: xiuyingt@yahoo.com, 23185962@qq.com, ldpyxa@sina.com

## Experimental

### Materials

In this work, zinc acetate (Zn(CH<sub>3</sub>COO)<sub>2</sub>·2H<sub>2</sub>O Hunan Xiangzhong Chemical Reagent Co., Ltd.), thioacetamide (C<sub>2</sub>H<sub>5</sub>NS, Hunan Huihong Chemical Reagent Co., Ltd.), soluble starch (Chendu Lichun Chemical Co., Ltd.) and concentrated sulfuric acid and nitric acid (Hunan Xiangzhong Chemical Reagent Co., Ltd.), dysprosium oxide (Dy<sub>2</sub>O<sub>3</sub>, Ganzhou Shunyuan Rare Earth Materials Co., Ltd.) have been used. All the aqueous solutions were prepared with distilled water. All reagents were of analytical reagent grade.

### Preparation of Dy<sup>3+</sup>-doped and undoped ZnS nanoparticles

In a typical procedure, the solution A was prepared by adding 4.38 g zinc acetate to 100 mL of the distilled water and then 1.50 g of thioacetamide was added to the 100 mL of distilled water, forming the solution B. 4 mL of 0.1 mol/L starch solution was added to the solution A and stirred for 30 min. Then, 1 mol%, 1.5 mol%, 2 mol%, 2.5 mol% and 3 mol% of dysprosium oxide (Dy<sub>2</sub>O<sub>3</sub>) was dissolved completely by adding an appropriate amount of concentrated nitric acid, respectively. And then they were added to the above solution A. The solution B was added to the above mixed solution drop by drop. Adjusting the pH value to 11 with NH<sub>3</sub>·H<sub>2</sub>O, the mixture was stirred for 30 min and moved into the microwave oven and heated at 80 °C for 7 min. The white precipitate was formed and recovered by centrifugation, washed 3 times with distilled water and washed 2 times with ethanol. The resultant product was dried at 80 °C for 12 hrs. The undoped ZnS nanoparticle was synthesized following the same procedure in the absence of the doping material.

### Characterization

The crystal phase composition of the samples were determined from XRD patterns recorded using a PANalytical X'Pert PRO X-ray diffractometer with Cu K<sub>α</sub> radiation (λ = 0.15418 nm). The crystal lattice structure of the sample was characterized by HR-TEM (JEM-2100, Japan). The morphology of samples was observed by FE-SEM (SU8000, Hitachi, Japan) operating at 10 kV. UV-Vis absorption spectra were recorded on UV-Vis spectrophotometer (Shimadzu, UV-2501, Japan). FTIR was performed in the region 4000-525 cm<sup>-1</sup> using Nicolet iS50 FT-IR spectrometer from Thermo Scientific. The PL spectra were obtained on Hitachi F-7000 FL spectrometer.

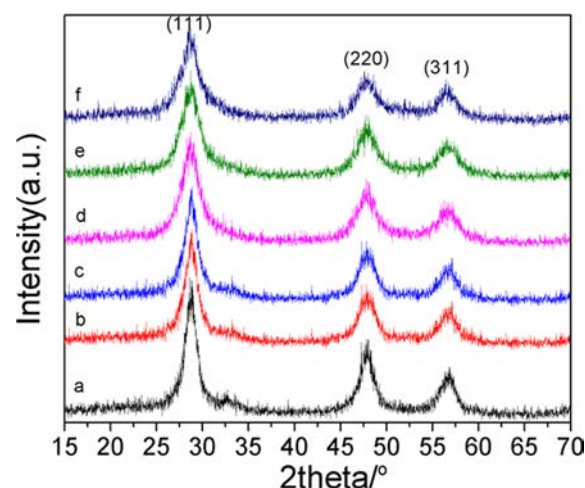
## Results and Discussion

Fig. 1 shows XRD spectra of undoped and Dy<sup>3+</sup>-doped ZnS samples (a, 0%; b, 1%; c, 1.5%; d, 2%; e, 2.5% and f, 3.0%). XRD curves are listed longitudinally with

the lowest concentration of Dy<sup>3+</sup> ions at the bottom. For all samples, there are three major diffraction peaks at 2θ around 29, 48 and 57 °, which correspond to the (111), (220) and (311) planes of ZnS with a ZB structure (JCPDS No. 05-0566). The structural parameters calculated by using Jade 6.5 software are showed in Table 1. Additional impurity phases due to Dy substitution are not observed in the XRD patterns with in the detection limit of the instrument. In the present work, we observe that the diffraction peak of (111) is slightly shifted to lower angles as the doping concentration increases. This is due to the bigger radius of Dy<sup>3+</sup> (0.091 nm) compared to that of Zn<sup>2+</sup> (0.074 nm), which has entered into the ZnS lattice substitutionally [18]. The values of the (111) interplanar spacing of all samples are in the range of 0.3101-0.3120 nm. Light variation in the lattice parameters of doped samples when compared to pure ZnS is found and the estimated values of the lattice parameter are in the range of 0.5373-0.5404 nm. The broadening diffraction peaks suggest that the size of all samples is on the nanoscale [17]. The average crystallite size can be estimated to be about in the range of 3.6-5.7 nm by Scherrer formula [38, 39, 41]:

$$D_{hkl} = \frac{k\lambda}{\beta_{hkl}\cos\theta} \quad (1)$$

where  $D_{hkl}$  is the mean crystallite size,  $\lambda$  is the



**Fig. 1.** XRD spectra of undoped and Dy<sup>3+</sup>-doped ZnS samples (a, 0%; b, 1%; c, 1.5%; d, 2%; e, 2.5% and f, 3.0%).

**Table 1.** Structural parameters of undoped and Dy<sup>3+</sup> doped ZnS samples.

Ratio	2θ <sub>(111)</sub> /°	d <sub>(111)</sub> /nm	D <sub>(111)</sub> /nm	a = b = c /nm
0%	28.9	0.3101	5.7	0.5372
1.0%	28.8	0.3102	5.7	0.5373
1.5%	28.5	0.3112	4.3	0.5388
2.0%	28.5	0.3112	3.6	0.5391
2.5%	28.4	0.3120	4.1	0.5404
3.0%	28.6	0.3116	3.9	0.5397

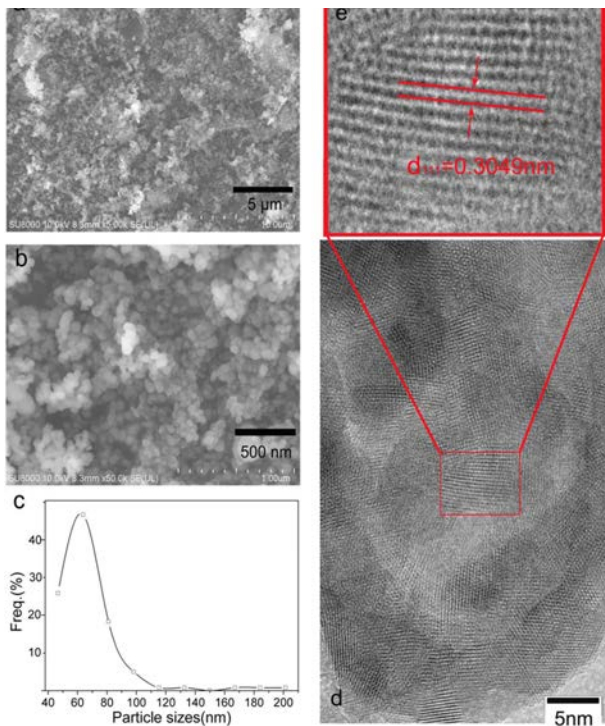


**Fig. 2.** A low and high magnification SEM (a and b), HR-TEM (d and e) images and distribution (c) of particle size of the typical ZnS sample with a  $\text{Dy}^{3+}$ -doped concentration of 1.0%.

wavelength of X-ray radiation (Cu  $K_{\alpha}$  radiation,  $\lambda = 0.15418$  nm),  $k_1$  is the shape factor and usually taken as 0.896,  $\beta_{\text{hk}}$  is the full width at half maximum (FWHM), after subtraction of equipment broadening, and  $\theta$  is the Bragg angle. Tab.1 also reveals that introducing  $\text{Dy}^{3+}$  ions inhibit growth of crystallite size to a certain extent.

Fig. 2(a) shows a low magnification SEM image of the  $\text{Dy}^{3+}$ -doped ZnS sample with the  $\text{Dy}^{3+}$  concentration of 1.0%. The particle size is relatively small and there are some agglomerations to a certain degree, due to higher special surface area of the nanoparticles. Fig. 2(b) shows a high magnification SEM image of the  $\text{Dy}^{3+}$ -doped ZnS sample with the  $\text{Dy}^{3+}$  concentration of 1.0%. It can be revealed that the morphology of ZnS nanoparticles is approximately spherical structure, wherein the particle size is in the range of about  $\sim 40\sim 210$  nm. Fig. 2(c) give the distribution of particle size of the  $\text{Dy}^{3+}$ -doped ZnS sample with the  $\text{Dy}^{3+}$  concentration of 1.0%. As can be seen, the particle size is in a narrow distribution centered at  $\sim 68$  nm. The minimum particle size of the sample is  $\sim 4$  nm and the maximum particle size of the sample is  $\sim 210$  nm. The result is not consistent with that from XRD patterns. Since the particles consist of a large number of crystallites, the particle size obtained using SEM is expected to be greater than that obtained using Scherer Formula, which gives the crystallite size. Figs. 2(d) and 2(e) show HRTEM images of the  $\text{Dy}^{3+}$ -doped ZnS sample with the  $\text{Dy}^{3+}$  concentration of 1.0%. Figs. 2(d) and 2(e) give the crystalline lattice structure of the

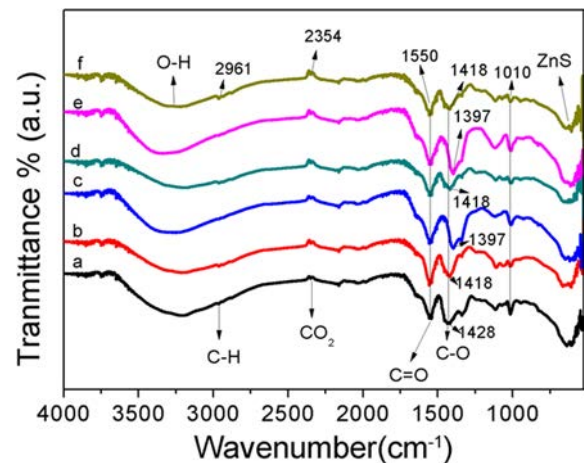


**Fig. 3.** FTIR spectra of undoped and  $\text{Dy}^{3+}$ -doped ZnS samples (a, 0%; b, 1%; c, 1.5%; d, 2%; e, 2.5% and f, 3.0%).

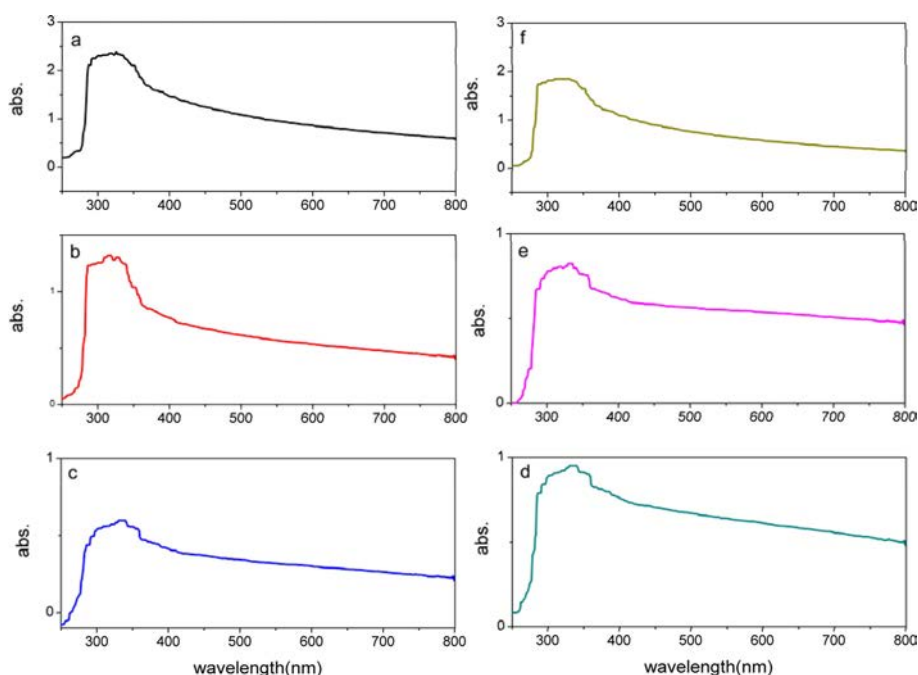
sample. As can be shown, the value of (111) interplanar spacing of the sample is 0.3049 nm, similar to the result of XRD (0.3102 nm).

Fig. 3 shows the FTIR spectra of undoped and  $\text{Dy}^{3+}$ -doped ZnS nanoparticles (a, 0%; b, 1%; c, 1.5%; d, 2%; e, 2.5% and f, 3.0%) prepared with starch as a bio-templete. It can be seen that the bands appearing at 662 and 602  $\text{cm}^{-1}$  are due to Zn-S vibration. The broad bands at 3000-3600  $\text{cm}^{-1}$  are attributed to -OH stretching vibrations. The bands at 2961  $\text{cm}^{-1}$  are assigned to stretching vibrations of C-H. The bands at 2354  $\text{cm}^{-1}$  are assigned to  $\text{CO}_2$ . The peaks observed at 1,550  $\text{cm}^{-1}$  are attributed to stretching vibration of C = O and the bands at 1428  $\text{cm}^{-1}$  are assigned to C-O. With increasing  $\text{Dy}^{3+}$ -doped concentration of ZnS samples, the bands at 1428  $\text{cm}^{-1}$  were shifted to the bands at 1397 and 1418  $\text{cm}^{-1}$ , due to the presence of  $\text{Dy}^{3+}$  ion in ZnS lattice site 2]. The characteristic peaks at 1010  $\text{cm}^{-1}$  are attributed to C-O bond stretching vibration of the C-O-C group in the anhydroglucose ring of starch [39].

Fig. 4 shows the UV-Vis spectra of undoped and  $\text{Dy}^{3+}$ -doped ZnS nanoparticles (a, 0%; b, 1%; c, 1.5%; d, 2%; e, 2.5% and f, 3.0%). The broad absorption bands centered at  $\sim 315\text{-}320$  nm are in the range of 250-450 nm. With the increase of  $\text{Dy}^{3+}$ -doped concentration of ZnS samples, the absorpton peaks are changed slightly, indicating that the energy band structure is tailored obscurely by the addition of  $\text{Dy}^{3+}$  into the ZnS matrix. The band gap energy ( $E_g$ ) can be evaluated by using Tauc's formula [38, 39, 42]:

$$(\alpha h\nu)^{1/n} = A(h\nu - E_g) \quad (2)$$

where  $\alpha$  is the absorption coefficient,  $h\nu$  is the discrete photoenergy,  $A$  is a constant,  $E_g$  is the band gap energy and  $n$  is equal to 1/2 for direct transition and 2 for indirect transition. The plots of  $(\alpha h\nu)^2$  versus  $h\nu$  of ZnS samples with different  $\text{Dy}^{3+}$ -doped concentrations based on the direct transition are shown in Fig. 5. The values



**Fig. 4.** UV-vis spectra of undoped and  $\text{Dy}^{3+}$ -doped ZnS samples (a, 0%; b, 1%; c, 1.5%; d, 2%; e, 2.5% and f, 3.0%).

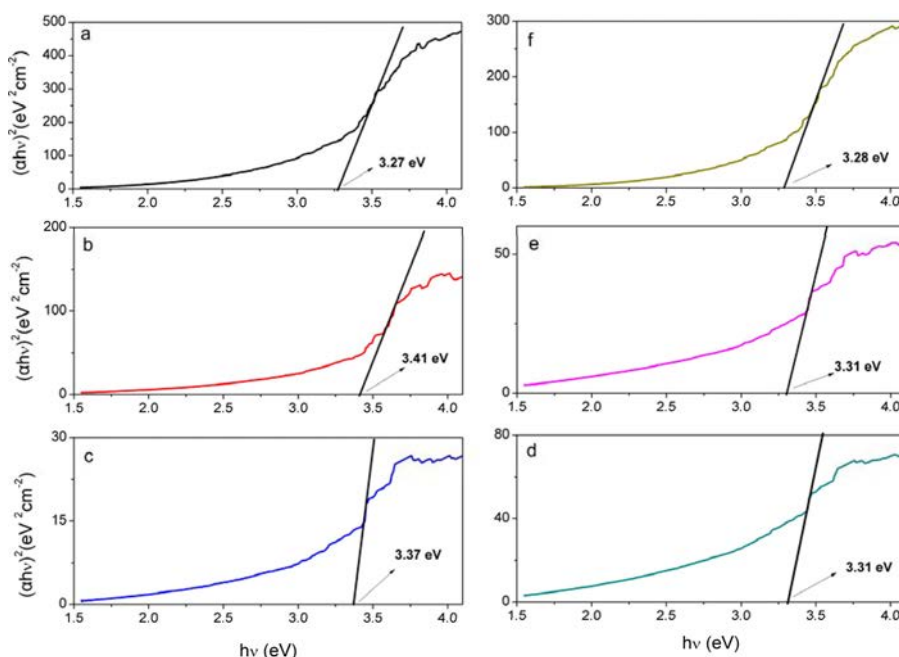


**Fig. 5.** The plots of versus of undoped and  $\text{Dy}^{3+}$ -doped ZnS samples (a, 0%; b, 1%; c, 1.5%; d, 2%; e, 2.5% and f, 3.0%).

of  $h\nu$  extrapolated to  $\alpha=0$  give the adsorption edge energies of undoped and  $\text{Dy}^{3+}$ -doped ZnS nanoparticles (a, 0%; b, 1%; c, 1.5%; d, 2%; e, 2.5% and f, 3.0%) which correspond to 3.27 eV, 3.41 eV, 3.37 eV, 3.31 eV, 3.31 eV and 3.28 eV. The band gap energy values of samples are apparently lower than the reference value ( $\sim 3.72$  eV), beneficial for the photo-catalytic application [43]. With increase of  $\text{Dy}^{3+}$ -doped concentration of ZnS samples, the band gap energy values are changed slightly, revealing that the energy band structures are

tailor slightly due to the injection of  $\text{Dy}^{3+}$  and doping  $\text{Dy}^{3+}$  inhibit the grow of particle size to a certain content.

The PL measurement of undoped and  $\text{Dy}^{3+}$ -doped ZnS nanoparticles was carried out with a Xe lamp at 320 nm excitation at room temperature. The PL emission spectra of undoped and  $\text{Dy}^{3+}$ -doped ZnS nanoparticles are shown in Fig. 6. The weak and narrow bands centered at  $\sim 360$  nm and the strong and broad emission bands centered at  $\sim 420$  nm and  $\sim 500$  nm has

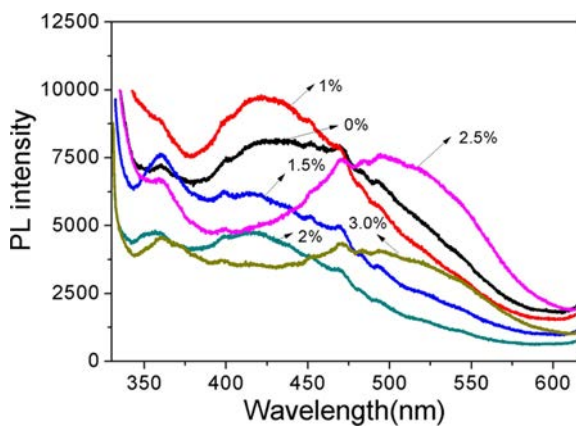


Fig. 6. PL spectra of undoped and Dy<sup>3+</sup>-doped ZnS samples.

been observed. In most cases, the band in the range of 340-380 nm is attributed to the polysaccharide from starch [39]. The ZnS nanostructures reported previously have PL emission with band in the range of 400-450 nm that originates from the surface defect states such as sulfur vacancies and with band centered around 500 nm that originates from the self-activated zinc vacancies of the ZnS nanostructures [44]. The band centered at 484 nm is ascribed to the  ${}^4F_{9/2}$ - ${}^6H_{15/2}$  transition in the emission spectrum [18]. Therefore, the band at 360 nm is attributed to the polysaccharide from starch and the strong and broad emission at  $\sim 20$  nm is attributed to the sulfur vacancies in ZnS nanoparticles. The broad band centered at  $\sim 500$  nm is attributed to the self-activated zinc vacancies of the ZnS nanoparticles and the  ${}^4F_{9/2}$ - ${}^6H_{15/2}$  transition of Dy<sup>3+</sup> ions.

It is interesting to note from Fig. 6 that the intensities of the peak at 420 nm in the PL emission increases firstly and then decreases with increasing Dy<sup>3+</sup>-doped concentrations. The emission peak of the sample with Dy<sup>3+</sup>-doped concentration of 1% is highest. When the Dy<sup>3+</sup>-doped concentration is 2.5%, the broad band at  $\sim 420$  nm disappears and another broad band at  $\sim 500$  nm appears. When the Dy<sup>3+</sup>-doped concentration is 3%, the intensity of the band at  $\sim 500$  nm lessens, attributed to concentration quenching. Compared with undoped ZnS sample, the sample with Dy<sup>3+</sup>-doped concentration of 1.0% presents higher sulfur vacancies than other samples according to intensity of the emission peaks. Because the crystal growth in the starch and microwave-assisted process is very rapid and the structure defects are inevitably, we reasonably believe that the blue luminescence is associated with the defect-related emission of the ZnS host. The broad band with blue-green emission at  $\sim 500$  nm, in our case, indicates a considerable number of zinc vacancies to impart green emission and  ${}^4F_{9/2}$ - ${}^6H_{15/2}$  transitions of Dy<sup>3+</sup> ions to impart blue emission.

## Conclusions

Dy<sup>3+</sup>-doped ZnS nanoparticles have been synthesized

using a starch and microwave-assisted approach. Surface morphology of Dy<sup>3+</sup>-doped ZnS nanoparticles is approximately spherical structure and a narrow distribution is centered at  $\sim 68$  nm. XRD studies showed that samples of all had ZB structure. FTIR spectra showed that with increasing Dy<sup>3+</sup>-doped concentration of ZnS samples, the bands at  $1428\text{ cm}^{-1}$  were shifted to the bands at  $1397$  and  $1418\text{ cm}^{-1}$ , due to the presence of Dy<sup>3+</sup> ion in ZnS lattice site. From UV-Vis absorption spectra, the band gap energy values of samples are apparently lower than the reference value ( $\sim 3.72$  eV), and this will be beneficial for the photo-catalytic application. With increase of Dy<sup>3+</sup>-doped concentrations, enhanced PL was observed at 1%, attributed to the sulfur vacancies. The broad band with blue-green emission at  $\sim 500$  nm was observed, indicating a considerable number of zinc vacancies to impart green emission and  ${}^4F_{9/2}$ - ${}^6H_{15/2}$  transitions of Dy<sup>3+</sup> ions to impart blue emission.

## Acknowledgments

Projects of Scientific Research Fund of Hunan Provincial Education Department (Grant No. 14A076, 14C0607), Natural Science Foundation of Hunan Province (Grant No. 2016JJ4044) and Hunan Provincial Key Laboratory of Fine Ceramics and Powder Materials (Grant No. 2016TP1028) are greatly appreciated.

## References

1. X. Xu, L. Hu, N. Gao, et al., *Adv. Funct. Mater.* 25 (2015) 445-454.
2. G. Murugadoss, M.R. Kumar, *Appl. Nanosci.* 4 (2014) 67-75.
3. X. Fang, T. Zhai, U.K. Gautam, et al., *Prog. Mater. Sci.* 56 (2011) 175-287.
4. R. Chauhan, A. Kumar, R.P. Chaudhary, *J. Lumin.* 145 (2014) 6-12.
5. Y. I. Choi, S. Lee, S. K. Kim, et al., *J. Alloys Compd.* 675 (2016) 46-56.
6. R. Sarkar, C. S. Tiwary, P. Kumbhakar, et al., *Physica E* 40 (2008) 3115-3120.
7. R. Chauhan, A. Kumar, R.P. Chaudhary, *Spectrochim Acta A Mol. Biomol. Spectrosc.* 113 (2013) 250-256.
8. P. Yang, M. Lü, D. Xü, et al., *Appl. Phys. A* 74 (2002) 257-259.
9. Z. Chen, X.X. Li, N. Chen, et al., *Mater. Sci. Eng. B* 177 (2012) 337-340.
10. P. Yang, M. Lü, D. Xü, et al., *Chem. Phys. Lett.* 336 (2001) 76-80.
11. B. Poornaprakash, U. Chalapathi, M. Reddeppa, et al., *Superlattice. Microst.* 97 (2016) 104-109.
12. G. Murugadoss, *J. Lumin.* 132 (2012) 2043-2048.
13. M. Mall, L. Kumar, *J. Lumin.* 130 (2010): 660-665.
14. Y. Chen, G.F. Huang, W. Q. Huang, et al., *Appl. Phys. A* 108 (2012) 895-900.
15. B. Poornaprakash, P.T. Poojitha, U. Chalapathi, et al., *Mater. Lett.* 181 (2016) 227-230.
16. W. Chen, J.O. Malm, V. Zwiller, et al., *Phys. Rev. B* 61 (2000) 11021-11024.

17. B. Poornaprakash, P.T. Poojitha, U. Chalapathi, et al., *Ceram. Int.* 42 (2016) 8092-8097.
18. K. Pillai, L.M. Sikkhwihilu, T.K. Hillie, *Mater. Chem. Phys.* 120 (2010) 619-624.
19. X. Fang, Y. Bando, C. Ye, et al., *J. Phys. Chem. C* 111 (2007) 8469-8474.
20. D. Yuvaraj, M. Sathyanarayanan, K.N. Rao, *J. Nanosci. Nanotech.* 14 (2014) 4500-4505.
21. X. Fang, C. Ye, X. Peng, et al., *J. Cryst. Growth* 263 (2004) 263-268.
22. H. Zhang, S. Zhang, S. Pan, et al., *Nanotechnology* 15 (2004) 945-948.
23. X. Xu, L. Hu, N. Gao, et al., *Adv. Funct. Mater.* 25 (2015) 445-454.
24. N. Shanmugam, S. Cholan, N. Kannadasan, et al., *Solid State Sci.* 28 (2014) 55-60.
25. S. Iravani, *Green Chem.* 13 (2011) 2638-2650.
26. X. Tian, W. He, J. Cui, et al., *J. Colloid Interface Sci.* 343 (2010) 344-349.
27. P. Mishra, R.S. Yadav, A.C. Pandey, *Ultrason. Sonochem.* 17 (2010) 560-565.
28. J. Han, H. Su, J. Xu, et al., *J. Nanopart. Res.* 14 (2012) 726-735.
29. T. Prakash, R. Jayaprakash, D. Sathya Raj, et al., *Sens. Actuators B Chem.* 176 (2013) 560-568.
30. N.C. Seeman, *Nature* 421 (2003) 427-431.
31. X. Lin, M. Wu, D. Wu, et al., *Green Chem.* 13 (2011) 283-287.
32. A. Cai, Y. Wang, S. Xing, et al., *Ceram. Int.* 38 (2012) 5265-5270.
33. X. Gao, H. Matsui, *Adv. Mater.* 17 (2005) 2037-2050.
34. F. Cao, D.X. Li, *Biomed. Mater.* 4 (2009) 025009-025014.
35. A.K. Jha, V. Kumar, K. Prasad, *J. Bionanosci.* 5 (2011) 162-166.
36. D. Ramimoghadam, M.Z.B. Hussein, Y.H. Taufiq-Yap, *Chem. Cent. J.* 7 (2013) 136-145.
37. Q. Dong, H. Su, C. Zhang, et al., *Chem. Eng. J.* 137 (2008) 428-435.
38. X. Tian, J. Wen, J. Hu, et al., *Solid State Sci.* 59 (2016) 39-43.
39. X. Tian, J. Wen, S. Wang, et al., *Mater. Res. Bull.* 77 (2016) 279-283.
40. J. Zhu, M. Zhou, J. Xu, et al., *Mater. Lett.* 47(2001) 25-29.
41. D. Sun, Y. Du, X. Tian, et al., *Mater. Res. Bull.* 60 (2014) 704-708.
42. K.J. Sreeram, M. Nidhin, B.U. Nair, *Bull. Mater. Sci.* 31 (2008) 937-942.
43. W.B. Soltan, M. Mbarki, S. Ammar, et al., *Opt. Mater.* 54 (2016) 139-146.
44. D. A. Reddy, D. H. Kim, S. J. Rhee, et al., *Nanoscale Res. Lett.* 9 (2014) 1-8.